

Electric Polarization Induced by a Proper Helical Magnetic Ordering in a Delafossite Multiferroic $\text{CuFe}_{1-x}\text{Al}_x\text{O}_2$

T. Nakaajima,^{1,*} S. Mitsuda,¹ S. Kanetsuki,¹ K. Tanaka,¹ K. Fujii,¹ N. Terada,² M. Soda,³ M. Matsuura,³ and K. Hirota³

¹*Department of Physics, Faculty of Science, Tokyo University of Science, Tokyo 162-8601, Japan*

²*ICYS, National Institute for Materials Science, Ibaraki 305-0044, Japan*

³*Institute for Solid State Physics, University of Tokyo, Kashiwa 277-8581, Japan*

(Dated: July 13, 2007, **preprint**)

Multiferroic $\text{CuFe}_{1-x}\text{Al}_x\text{O}_2$ ($x = 0.02$) exhibits a ferroelectric ordering accompanied by a proper helical magnetic ordering below $T = 7\text{K}$ under zero magnetic field. By polarized neutron diffraction and pyroelectric measurements, we have revealed a one-to-one correspondence between the spin helicity and the direction of the spontaneous electric polarization. This result indicates that the spin helicity of the proper helical magnetic ordering is essential for the ferroelectricity in $\text{CuFe}_{1-x}\text{Al}_x\text{O}_2$. The induction of the electric polarization by the proper helical magnetic ordering is, however, cannot be explained by the Katsura-Nagaosa-Balatsky model, which successfully explains the ferroelectricity in the recently explored ferroelectric helimagnets, such as TbMnO_3 . We thus conclude that $\text{CuFe}_{1-x}\text{Al}_x\text{O}_2$ is a new class of magnetic ferroelectrics.

PACS numbers: 75.80.+q, 75.25.+z, 77.80.-e

Novel types of couplings between dielectric property and magnetism, which produce colossal magnetoelectric (ME) effects, have been extensively investigated since a gigantic ME effect was discovered in RMnO_3 (R is a rare earth material) [1]. Among several types of couplings between spins and electric polarizations, a ferroelectricity induced by noncollinear spin arrangements has been most widely investigated experimentally and theoretically [2, 3, 4, 5, 6, 7, 8]. Katsura, Nagaosa and Baratsky (KNB) proposed that the local electric dipole moment \mathbf{p} , which arises between neighboring two spins \mathbf{S}_i and \mathbf{S}_{i+1} , can be described in the form of $\mathbf{p} \propto \mathbf{e}_{i,i+1} \times (\mathbf{S}_i \times \mathbf{S}_{i+1})$, where $\mathbf{e}_{i,i+1}$ is a unit vector connecting two spins [2]. This formula successfully explains the ferroelectric property in cycloidal or conical magnetic orderings of some transition metal oxides, such as RMnO_3 ($R=\text{Tb}, \text{Tb}_{1-x}\text{Dy}_x$), $\text{Ni}_3\text{V}_2\text{O}_8$, MnWO_4 and CoCr_2O_4 [4, 5, 6, 7, 8]. Moreover, a recent polarized neutron diffraction study on TbMnO_3 demonstrated that the spin helicity, clockwise or counterclockwise, correlates with the direction of the electric polarization, as predicted in the formula [9]. It is, however, recently reported that ferroelectricity in a helical magnetic ordering of a delafossite multiferroic $\text{CuFe}_{1-x}\text{Al}_x\text{O}_2$ cannot be explained by the above formula [10]. Therefore, $\text{CuFe}_{1-x}\text{Al}_x\text{O}_2$ provides an opportunity to explore another type of spin-polarization coupling.

CuFeO_2 , which is one of model materials of a triangular lattice antiferromagnet, has been extensively investigated as a geometrically frustrated spin system for last fifteen years [11, 12, 13]. The ground state of CuFeO_2 is a collinear commensurate 4-sublattice ($\uparrow\uparrow\downarrow\downarrow$) state with the magnetic moments along the c axis, which is normal to the triangular lattice layers, in spite of the Heisenberg spin character expected from the electronic configuration

of Fe^{3+} ($S = \frac{5}{2}, L = 0$). When a magnetic field is applied along the c axis at low temperature, CuFeO_2 exhibits a multi-step magnetization process consisting of several magnetization plateaus and slopes, which is accompanied by stepwise changes of lattice constants [14, 15]. Since Kimura and co-workers discovered a spontaneous electric polarization in the first field-induced phase of CuFeO_2 , which emerges along the direction perpendicular to the c axis [16], CuFeO_2 has also been investigated as a candidate of novel multiferroic materials. Recent studies on the slightly diluted system $\text{CuFe}_{1-x}\text{Al}_x\text{O}_2$ showed that only a few percent dilution of Fe^{3+} sites with nonmagnetic Al^{3+} ions considerably reduces the transition field from the 4-sublattice phase to the field-induced ferroelectric phase. Moreover, the ferroelectric phase shows

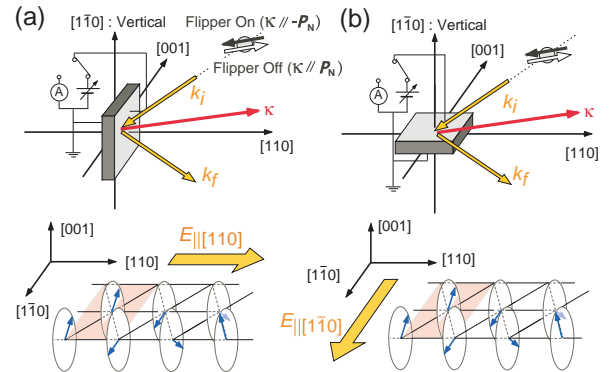


FIG. 1: (Color online) Schematic illustrations of the experimental configurations and the relationship between the direction of the poling electric field E and the proper helical magnetic structure in the FEIC phase for (a) the $E_{\parallel[110]}$ sample and (b) the $E_{\parallel[1\bar{1}0]}$ sample.

up even under zero field in the concentration region of $0.014 < x < 0.030$ [17, 18, 19]. Quite recently, the magnetic structure in the ferroelectric phase was elucidated to be an antiferromagnetically-stacked proper helical structure with an incommensurate propagation wave vector $(q, q, 0)$ where $q \sim 0.21$ [10]. In this letter, we refer to this ferroelectric phase as ferroelectric incommensurate (FEIC) phase. This magnetic structure, however, cannot lead to a finite uniform electric polarization through the formula $\mathbf{p} \propto \mathbf{e}_{i,i+1} \times (\mathbf{S}_i \times \mathbf{S}_{i+1})$, because the direction of $\mathbf{e}_{i,i+1}$ is parallel to the direction of $\mathbf{S}_i \times \mathbf{S}_{i+1}$ in average. Nevertheless, the spin helicity, a right-handed (RH) or left-handed (LH) proper helical arrangement of spins, is expected to correlate with the direction of the electric polarization, because space inversion operation flips the spin helicity, as well as the direction of electric polarization. In present work, we thus performed polarized neutron diffraction and pyroelectric measurements using $\text{CuFe}_{1-x}\text{Al}_x\text{O}_2$ samples with $x = 0.02$, which exhibits the ferroelectric ordering below $T = 7\text{K}$, in order to elucidate the relationship between the spin helicity and the electric polarization.

A single crystal of $\text{CuFe}_{1-x}\text{Al}_x\text{O}_2$ with $x = 0.02$ of nominal composition was prepared by the floating zone technique [20], and cut into two pieces with disk shapes; one of them has the widest surface normal to the $[110]$ axis ($E_{\parallel[110]}$ sample), the other has that normal to the $[\bar{1}\bar{1}0]$ axis ($E_{\parallel[\bar{1}\bar{1}0]}$ sample). The experimental configurations for these samples are illustrated in Figs. 1(a) and (b). Silver paste was pasted on the widest surface of each sample to make the electrodes. The polarized neutron diffraction measurements were carried out at the triple-axis neutron spectrometer PONTA installed by University of Tokyo at JRR-3 in Japan Atomic Energy Agency. The incident polarized neutron with the energy of 34.05 meV was obtained by a Heusler (111) monochromator. The flipping ratio of the polarized neutron beam was 19.0, and the polarization vector of the incident neutron, \mathbf{p}_N , was set to be parallel (or antiparallel) to the scattering vector, $\boldsymbol{\kappa}$, by a guide-field of a helmholtz coil and a spin flipper. The collimation was $40'-40'-40'-40'$, and a pyrolytic graphite analyzer was employed. The sample was mounted in a pumped ^4He cryostat with the (hhl) scattering plane. Note that, in the present experiment, we employed a conventional hexagonal basis as was in the previous works, while $\text{CuFe}_{1-x}\text{Al}_x\text{O}_2$ originally has a trigonal (rhombohedral) crystal structure. The definition of the hexagonal basis is shown in Fig. 2(a). For the measurements of the spontaneous electric polarization \mathbf{P} , pyroelectric current was measured under zero electric field with increasing temperature, using an electrometer (Keithley 6517A). Before each neutron diffraction (or pyroelectric) measurement, we performed a proper cooling with applied electric field from 20K to 2K.

Before discussing the results of the present measurements, we briefly review the scattering cross section for

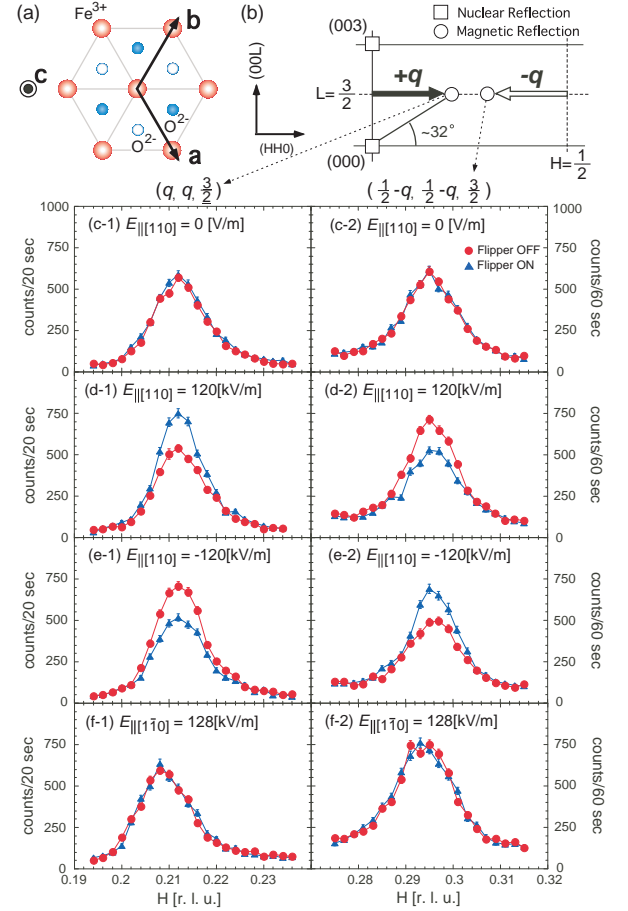


FIG. 2: (Color online) (a) The the hexagonal basis represented on the Fe^{3+} triangular lattice layer. Open and filled blue circles denote O^{2-} ions located above and below the Fe^{3+} layer, respectively. (b) The location of the magnetic reflections surveyed in present measurement in (HLL) zone. (c-1)-(f-2) The diffraction profiles of $(H, H, \frac{3}{2})$ reciprocal lattice scans for the $(q, q, \frac{3}{2})$ and $(\frac{1}{2}-q, \frac{1}{2}-q, \frac{3}{2})$ magnetic Bragg reflections at $T = 2\text{K}$ in the FEIC phase.

polarized neutrons. Let us assume that scattering system consists of RH- and LH-proper helical magnetic orderings with a propagation wave vector \mathbf{q} . According to the Blume's notation [21], the scattering cross section for a pair of magnetic satellite reflections located at $\boldsymbol{\tau} \pm \mathbf{q}$, where $\boldsymbol{\tau}$ is a reciprocal lattice vector, is described as follows:

$$\left(\frac{d\sigma}{d\Omega}\right)_{\boldsymbol{\tau} \pm \mathbf{q}} \propto S(\boldsymbol{\kappa}) \{ (1 + (\hat{\mathbf{C}} \cdot \hat{\boldsymbol{\kappa}})^2) (V_{\text{RH}} + V_{\text{LH}}) \mp 2(\mathbf{p}_N \cdot \hat{\boldsymbol{\kappa}})(\hat{\mathbf{C}} \cdot \hat{\boldsymbol{\kappa}})(V_{\text{RH}} - V_{\text{LH}}) \}, \quad (1)$$

where $S(\boldsymbol{\kappa})$ is the factor depending on the magnetic structure factor, V_{RH} and V_{LH} are the volumes of the RH- and LH-helical orderings, respectively, $\hat{\boldsymbol{\kappa}}$ is a unit vector of $\boldsymbol{\kappa}$, $|\mathbf{p}_N| = 1$, and $\hat{\mathbf{C}}$ is a unit vector corresponding to the spin helicity, (referred as 'vector spin chi-

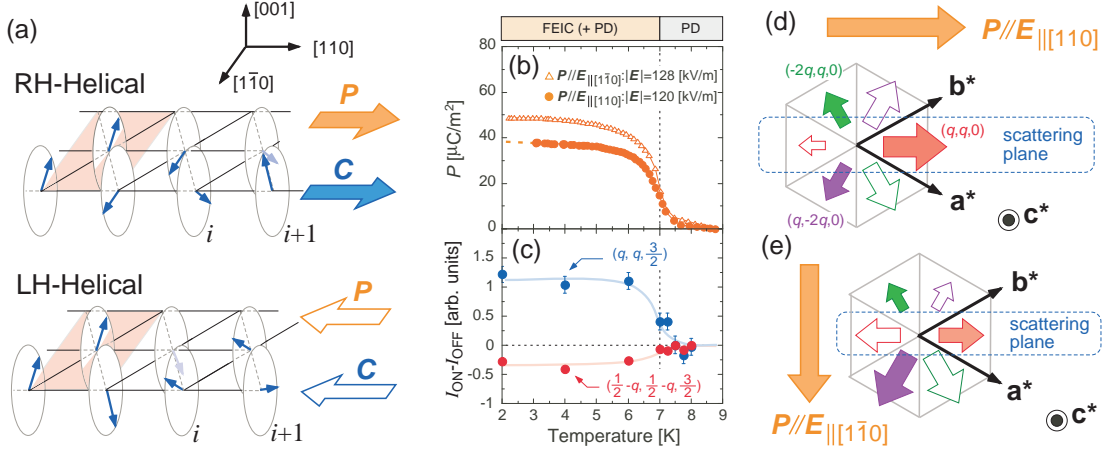


FIG. 3: (Color online) (a) The relationship between the spin helicity and the direction of the electric polarization. (b) The temperature variations of the electric polarization along the $[110]$ and $[1\bar{1}0]$ axes measured after cooling with the poling electric field parallel to the $[110]$ and $[1\bar{1}0]$ directions, respectively. (c) The temperature dependence of $I_{ON} - I_{OFF}$ measured on heating after a cooling with a poling electric field (120 kV/m) parallel to $[110]$ axis. The schematic drawings of the distributions of the RH- (filled arrows) and LH- (open arrows) helical orderings among magnetic domains with three equivalent propagation wave vectors $(q, q, 0)$, $(-2q, q, 0)$ and $(q, -2q, 0)$, when the macroscopic electric polarization emerges along (d) the $[110]$ axis and (e) the $[1\bar{1}0]$ axis. The fractions of the RH- (or LH-) helical orderings are represented by the sizes of arrows.

rality' in Ref.[9]) which is defined so that $\mathbf{S}_i, \mathbf{S}_{i+1}$ and \mathbf{C} in this order form a right-handed coordinate system (see Fig. 3(a)). Note that the above expression of the scattering cross section includes both the 'spin-flip' and 'non spin-flip' scatterings, and thus polarization analysis for scattered neutrons is not necessary. In the present experiment, \mathbf{C} is parallel (antiparallel) to the $[110]$ direction for the RH- (LH-) proper helical ordering, and the cross sections of two magnetic Bragg reflections at $(q, q, \frac{3}{2})$ and $(\frac{1}{2} - q, \frac{1}{2} - q, \frac{3}{2})$, which are mainly surveyed in the present measurements, correspond to $(d\sigma/d\Omega)\boldsymbol{\tau} + \mathbf{q}$ and $(d\sigma/d\Omega)\boldsymbol{\tau} - \mathbf{q}$, respectively (see Fig. 2(b)). In this case, the imbalance between V_{RH} and V_{LH} is expressed as following:

$$\frac{V_{RH} - V_{LH}}{V_{RH} + V_{LH}} = A(\boldsymbol{\kappa}) \left(\frac{I_{ON} - I_{OFF}}{I_{ON} + I_{OFF}} \right), \quad (2)$$

where I_{ON} and I_{OFF} are the intensities of a magnetic Bragg reflection measured when the spin flipper is on ($\mathbf{p}_N \parallel -\boldsymbol{\kappa}$) and off ($\mathbf{p}_N \parallel \boldsymbol{\kappa}$), respectively. The values of the proportional constant $A(\boldsymbol{\kappa})$ for the $(q, q, \frac{3}{2})$ and $(\frac{1}{2} - q, \frac{1}{2} - q, \frac{3}{2})$ magnetic reflections are approximately 1 and -1 , respectively.

In Fig. 2, we now show typical diffraction profiles of magnetic reflections in the FEIC phase ($T = 2\text{K}$). After cooling the $E_{\parallel[110]}$ sample under zero electric field, as shown in Figs. 2 (c-1) and (c-2), there was no difference between I_{ON} and I_{OFF} for both of the $(q, q, \frac{3}{2})$ and $(\frac{1}{2} - q, \frac{1}{2} - q, \frac{3}{2})$ reflections. This result indicates that the fractions of the RH- and LH-helical magnetic orderings were equal to each other. After cooling the $E_{\parallel[110]}$ sample under a poling electric field (120 kV/m) parallel

to the $[110]$ direction, I_{ON} was greater than I_{OFF} for the $(q, q, \frac{3}{2})$ reflection, and this relationship between I_{ON} and I_{OFF} was reversed for the $(\frac{1}{2} - q, \frac{1}{2} - q, \frac{3}{2})$ reflection, as shown in Figs. 2(d-1) and (d-2). By a reversal of the direction of the poling electric field applied on cooling, this relationship between I_{ON} and I_{OFF} for each magnetic satellite was reversed, as shown in Figs. 2(e-1) and (e-2). No imbalance between I_{ON} and I_{OFF} , however, was observed for the $E_{\parallel[1\bar{1}0]}$ sample after cooling under the poling electric field (128 kV/m) parallel to the $[1\bar{1}0]$ direction, as shown in Figs. 2(f-1) and (f-2). These results show that the poling electric field along the $[110]$ axis induces an imbalance between the fractions of the RH- and LH-helical orderings, but the poling electric field along $[1\bar{1}0]$ axis does not. Taking account of the fact that the poling electric field along the $[110]$ axis also induces the macroscopic electric polarization along the $[110]$ axis (see Fig. 3(b)), we conclude that a proper helical magnetic ordering generates an electric polarization along the helical axis, and moreover, there is the one-to-one correspondence between the spin helicity and the direction of electric polarization, as illustrated in Fig. 3(a).

Although the poling electric field along the $[1\bar{1}0]$ axis also induces the macroscopic electric polarization along the $[1\bar{1}0]$ axis, as shown in Fig. 3(b), this can be ascribed to the existence of three magnetic domains reflecting the trigonal three-fold symmetry of the crystal structure (see Fig. 2(a)). When the electric polarization emerges along the $[1\bar{1}0]$ axis, the imbalance between the fractions of the RH- and LH-helical ordering must be induced in the domains out of the scattering plane, as illustrated in Fig. 3(e).

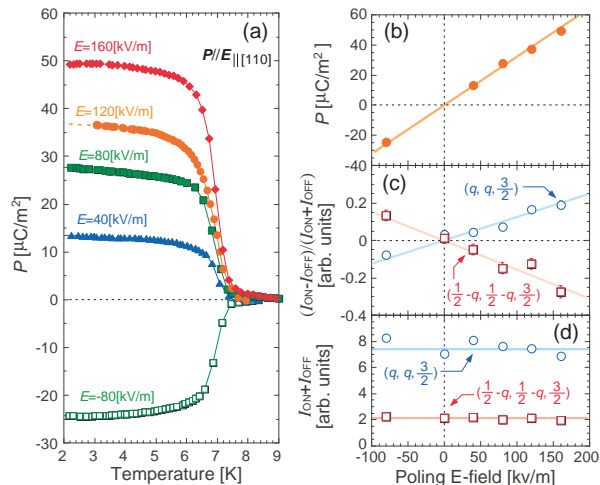


FIG. 4: (Color online) (a) Temperature variations of the electric polarization along the [110] axis measured after cooling under various poling electric fields along the [110] axis. The poling electric field dependence of (b) the spontaneous electric polarization, (c) $(I_{\text{ON}} - I_{\text{OFF}})/(I_{\text{ON}} + I_{\text{OFF}})$ and (d) $(I_{\text{ON}} + I_{\text{OFF}})$ at $T = 2\text{K}$. The colored solid lines are guides to eyes.

Figs. 4(a)-(c) show the poling electric field dependence of the spontaneous electric polarization and the imbalance between I_{ON} and I_{OFF} for the $E_{\parallel(110)}$ -sample. We found that both the magnitude of the electric polarization and the imbalance between I_{ON} and I_{OFF} at $T = 2\text{K}$ are proportional to the poling electric field applied on cooling. In addition, the temperature variation of $I_{\text{ON}} - I_{\text{OFF}}$, which was measured in a warming run under zero electric field after a cooling with the poling electric field parallel to the [110] axis, is similar to that of the spontaneous electric polarization, as shown in Figs. 3(c). These results apparently show that the macroscopic electric polarization arises from the ‘imbalance’ between the fractions of the RH- and LH-helical magnetic orderings. Note that the fractions of the RH- and LH-helical magnetic orderings, however, cannot be determined accurately in the present experiments, because the thermally induced partially disordered (PD) state, which has a collinear incommensurate magnetic structure with almost the same wave number as that of the FEIC magnetic ordering, is supposed to remain even in the FEIC phase owing to the pinning effect by nonmagnetic impurity ions [10, 19]. While the imbalance between I_{ON} and I_{OFF} apparently shows the poling electric field dependence as mentioned above, the sum of I_{ON} and I_{OFF} does not, as shown in Fig. 4(d). This means that the application of a poling electric field within $|E| < \sim 160$ kV/m does not affect the fractions of the three magnetic domains, whose propagation wave vectors are different to each other.

In summary, we performed polarized neutron diffrac-

tion and pyroelectric measurements on the delafossite multiferroic $\text{CuFe}_{1-x}\text{Al}_x\text{O}_2$ with $x = 0.02$, and demonstrated that the proper helical magnetic ordering of $\text{CuFe}_{1-x}\text{Al}_x\text{O}_2$ generates a spontaneous electric polarization parallel to the helical axis. This indicates that the local spin-polarization coupling in $\text{CuFe}_{1-x}\text{Al}_x\text{O}_2$ cannot be explained by the KNB-model ($\mathbf{p} \propto \mathbf{e}_{i,i+1} \times (\mathbf{S}_i \times \mathbf{S}_{i+1})$). Nevertheless, the results of the present study revealed a one-to-one correspondence between the spin helicity and the direction of the electric polarization, indicating that the spin helicity of the proper helical magnetic ordering is essential for the ferroelectricity in $\text{CuFe}_{1-x}\text{Al}_x\text{O}_2$. Quite recently, Arima proposed that a proper helical magnetic order can generate ferroelectricity through the variation in the metal-ligand hybridization with spin-orbit coupling [22]. The present results suggest that this mechanism is applicable to $\text{CuFe}_{1-x}\text{Al}_x\text{O}_2$. We thus conclude that $\text{CuFe}_{1-x}\text{Al}_x\text{O}_2$ is a new class of magnetic ferroelectrics, which will pave another way to design multiferroic materials.

We are grateful to T. Arima for fruitful discussions. The neutron diffraction measurement at JRR-3M was supported by ISSP of the University of Tokyo (PACS No. 7546B (5G:PONTA)). This work was supported by a Grant-in-Aid for Scientific Research (C), No. 19540377, from JSPS, Japan.

* Electronic address: E-mail address: nakajima@nsm-smac4.ph.kagu.tus

- [1] T. Kimura *et al.*, Nature (London) **426**, 55 (2003).
- [2] H. Katsura, N. Nagaosa and A. V. Balatsky, Phys. Rev. Lett. **95**, 057205 (2005).
- [3] M. Mostovoy, Phys. Rev. Lett. **96**, 067601 (2006).
- [4] M. Kenzelmann *et al.*, Phys. Rev. Lett. **95**, 087206 (2005).
- [5] T. Arima *et al.*, Phys. Rev. Lett. **96**, 097202 (2006).
- [6] G. Lawes *et al.*, Phys. Rev. Lett. **95**, 087205 (2005).
- [7] K. Taniguchi *et al.*, Phys. Rev. Lett. **97**, 097203 (2006).
- [8] Y. Yamasaki *et al.*, Phys. Rev. Lett. **96**, 207204 (2006).
- [9] Y. Yamasaki *et al.*, Phys. Rev. Lett. **98**, 147204 (2007).
- [10] T. Nakajima *et al.*, J. Phys. Soc. Jpn. **76**, 043709 (2007).
- [11] S. Mitsuda *et al.*, J. Phys. Soc. Jpn. **60**, 1885 (1991).
- [12] S. Mitsuda *et al.*, J. Phys. Soc. Jpn. **69**, 3513 (2000).
- [13] O. A. Petrenko *et al.*, Phys. Rev. B **62**, 8983 (2000).
- [14] N. Terada *et al.*, Phys. Rev. B **74**, 180404(R) (2006).
- [15] N. Terada *et al.*, Phys. Rev. B **75**, 224411 (2007).
- [16] T. Kimura, J. C. Lashley, and A. P. Ramirez, Phys. Rev. B **73**, 220401(R) (2006).
- [17] S. Kanetsuki *et al.*, J. Phys.: Condens. Matter **19**, 145244 (2007).
- [18] S. Seki *et al.*, Phys. Rev. B **75**, 100403(R) (2007).
- [19] N. Terada *et al.*, J. Phys. Soc. Jpn. **74**, 2604 (2005).
- [20] T. R. Zhao, M. Hasegawa and H. Takei, J. Cryst. Growth **166**, 408 (1996).
- [21] M. Blume, Phys. Rev. **130**, 1670 (1963).
- [22] T. Arima, J. Phys. Soc. Jpn. **76**, 073702 (2007).